AN ABSTRACT OF THE THESIS OF

Robert Broome for the Master of Science

in Oceanography presented on May 30, 1978

Title: SEDIMENT TRANSPORT BENEATH AN UNDULAR HYDRAULIC JUMP

Abstract Approved: Paul D. Komar

Field observations are made of the formation of backwash ripples on the beachface, formed by undular hydraulic jumps generated by backwash down the beach face colliding with wave bores. Measured ripple wavelengths range from set averages of 48 to 70 cm. Within a particular set of ripples there is a tendency for the spacing to decrease in the offshore direction. These field observations are compared with laboratory experiments where undular jumps are generated in a flume, and with a computer simulation model which models both the flow within an undular hydraulic jump and the resulting sediment transport which gives rise to the backwash ripples. The computer model involves a numerical solution of the Boussinesq equations which govern the fluid flow, and sediment transport equations which relate the sand transport rate to the local mean flow velocity. The computer model permits a study of the detailed time-history of the undular jump development and the formation of the backwash ripples. This model shows good agreement with the field observations of backwash ripples, predicting an offshore

decrease in their spacing as observed. The laboratory experiments showed a similar result so long as the Froude number of the supercritical flow before the jump occurs is small, on the order of 1.4. Differences between the computer model and experiments were small and arose principally from the neglect of internal friction and surface tension in the model. The study demonstrates the usefulness of the simultaneous application of computer simulation models and laboratory experiments to understand complex flow and sediment transport conditions such as occur on beaches.

SEDIMENT TRANSPORT BENEATH AN UNDULAR HYDRAULIC JUMP

by

Robert Broome

A THESIS

submitted to

Oregon State University

in partial fulfillment of
the requirements for the
degree of

Master of Science

Completed June 1978

Commencement June 1979

APPROVED:

Redacted for Privacy

Professor of Oceanography in Charge of Major

Redacted for Privacy

Acting Dean of School of Oceanography

Redacted for Privacy

Dean of Graduate School

Date thesis presented May 30, 1978

Typed by Cheryl M. Schurg for Robert Broome

ACKNOWLEDGEMENTS

I wish to thank Dr. Paul Komar for his help with this project. I also wish to thank the Milne Computer Center at OSU for necessary computer support for the computer model phase of this study.

This work is a result of research sponsored by the Oregon State University Sea Grant College Program, supported by NOAA Office of Sea Grant, Department of Commerce, under grant number 04-7-158-44085.

TABLE OF CONTENTS

	Page
INTRODUCTION	
Purpose and Scope of this Study	1
FIELD OBSERVATIONS AND MEASUREMENTS	5
Description of the Study Area	5
Observation of an Undular Hydraulic Jump	7
Kinds of Hydraulic Jumps	7
Measurements of an Undular Hydraulic Jump	8
THE COMPUTER SIMULATION MODEL	14
The Parameters of the Solution	15
Sediment Transport Equations	18
An Example of the Solution	20
Phase Relations of the Surface and Bed Profiles	24
DETERMINATION OF THE HORIZONTAL LENGTH SCALE ℓ	26
ℓ as a Function of $\bar{\lambda}$ and h_o	26
Comparison of Field Measurements with the Scaled Computer Results	29
LABORATORY EXPERIMENTS	30
Experimental Measurements of Velocity and Surface Height	32
Comparison of Experimental Results with the Computer Model	33
Description of the Experimental Results	33
CONCLUSIONS	36
BIBLIOGRAPHY	37
APPENDIX I	39
APPENDIX II	49

LIST OF FIGURES

Figure		Page
1	Backwash ripples at Agate Beach, Oregon.	2
2	An example of an undular hydraulic jump on a beach.	6
3	The three classes of hydraulic jumps.	9
4	Offshore variations in ripple wavelengths for field measurements.	13
5	A diagram of the symbols used to describe an undular hydraulic jump.	15
6	An example of the numerical solution of the Boussinesq equations with sediment transport.	20
7	The phase shift between the surface profile, the bed profile, the velocity and related quantities.	25
8	Offshore variations in wavelet wavelengths for the computer mode.	27
9	Experimental measurements of velocity and surface height for an undular hydraulic jump.	32
10	Vertical profile of the velocity beneath the first wavelet of an undular hydraulic jump.	34

LIST OF TABLES

Table		Page
I	Field measurements of backwash ripple spacing.	11

SEDIMENT TRANSPORT BENEATH AN UNDULAR HYDRAULIC JUMP

INTRODUCTION

Wave action on a beach forms a great variety of sedimentary structures in the sand. Among these structures are regular patterns of ripples known as *backwash ripples* (Figure 1). They are often made readily visible by selective sorting of sediments such that heavier and darker minerals are left in the troughs and the lighter quartz and feldspar sand grains form the crests. The wavelengths of backwash ripples generally range 30-70 cm. They are a distinctive class of ripples due to their low amplitudes compared to their wavelengths giving a ripple index (ratio of length to height) of 30 to 100, much larger than other types of ripples (Tanner, 1965). Backwash ripples are temporary structures in the sense that they persist on a beach during a falling tide only when subsequent waves fail to reach them. They are washed away on the next rising tide only to reform as the tide again recedes.

Little study has gone into the actual formation of backwash ripples, although it is generally recognized that they form when the backwash of a wave becomes supercritical (Froude number greater than unity) as it flows seaward down the beachface, giving rise to a hydraulic jump (Hayes, 1972, p. 344). The jump so produced may be an undular hydraulic jump with a series of undulations or wavelets forming on the water surface, the undulations in the water forming similar undulations or backwash ripples on the sand beneath.

Figure 1: Backwash ripples covering the beach face at Agate Beach, Oregon, at low tide. The ocean is to the left in the photo. These backwash ripples have been modified by swash action after their initial formation within undular hydraulic jumps, some of the sand of the crests having been carried over into adjacent seaward ripple troughs.

The purpose of this study is to understand the causes and flow characteristics of undular hydraulic jumps on beaches, and how they give rise to backwash ripples. Of special concern will be how the ripple geometry, mainly the spacings of the backwash ripples, relates to the flow in the hydraulic jump. The first step of this study is to undertake field observations of backwash ripples being formed, and to obtain measurements of the resulting ripple spacings. With these measurements as a guide we will then devise a computer model that describes the flow of water in an undular hydraulic jump. Measurements in undular hydraulic jumps in a laboratory flume are used to test the computer model and to properly scale the solutions. The computer flow model will then be used as a forcing function for a sediment transport model which will simulate the movement of sand beneath the undular hydraulic jump. As will be seen, this numerical model simulates the formation of backwash ripples, which can then be compared with real backwash ripples observed on the beaches. The numerical results thus give us a detailed time history of the formation of backwash ripples by an undular hydraulic jump. These results are then used to describe what the physical conditions were on the beach at the time the field measurements were taken.

Although the scope of this study is directed toward a better understanding of the formation of backwash ripples on a beach, undular hydraulic jumps also form in rivers and streams. This study can also give information on what is happening in these places. Conditions in

channels are more difficult to model; the flow conditions are steady for longer periods and there are side walls that may affect the flow. Under these conditions, the model described in this study may well fail; however, it is a good way to begin further study of such a flow regime in a channel.

FIELD OBSERVATIONS AND MEASUREMENTS

Observations of the formation of backwash ripples and measurements of their wavelengths were made at several beaches, but principally at Agate Beach, Oregon, 5 km north of Newport on the mid-Oregon coast. Due to the high concentration of heavy minerals in Agate Beach, the backwash ripples are very apparent (Figure 1). The exposed portion of beach face upon which the backwash ripples form has a uniform slope of about 0.01 . The beach is exposed directly to the full ocean waves which average 1-2 m significant height breaking waves in the summer, increasing to an average of 4 m in the winter with individual storms forming breakers of 6 to 7 m (Komar et al., 1976). Wave periods average 8 sec during the summer, increasing to 10 to 15 sec in the winter. Tides are mixed with a Spring tidal range of 3.5 m.

All of our observations substantiated that the backwash ripples are formed by the water undulations or wavelets of an undular hydraulic jump. A clear example of this occurring is shown in Figure 2. The upper photograph shows the undular hydraulic jump produced by the backwash running down the beach face colliding with a small incoming wave bore. The bottom photograph of Figure 2 shows the backwash ripples so produced. Backwash ripples do not form under each incoming wave bore, only when there has been a series of large bores which wash high upon the beach face. This causes a general flooding of the beach face followed by a long steady return back flow lasting up to a minute. This long return flow would then halt a sizeable incoming bore, producing

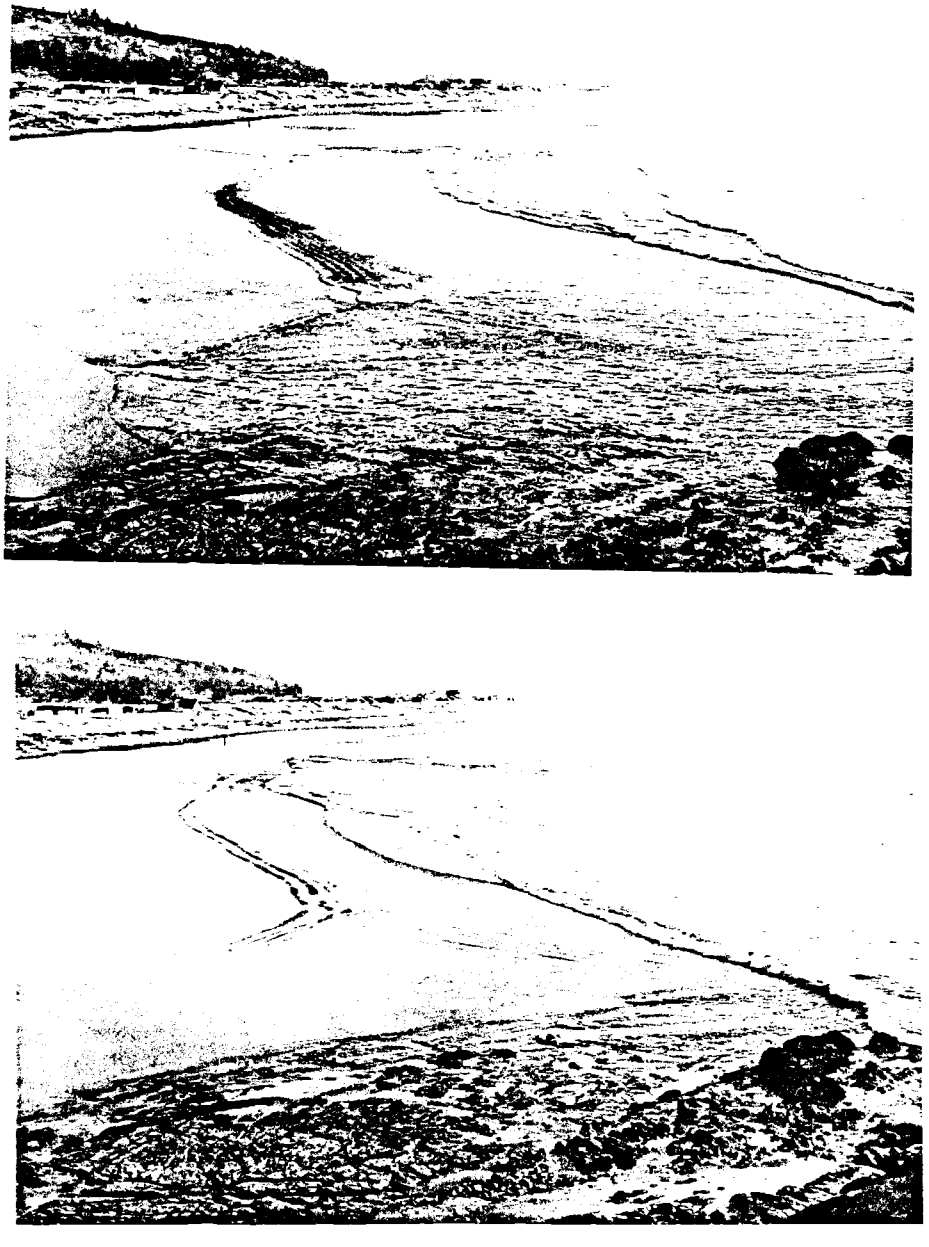

Figure 2: Successive photographs about 15 seconds apart, showing an undular hydraulic jump with five wavelets (above), and then the backwash ripples produced by those wavelets (below). Photos from Cape Kiwanda, Oregon.

an undular hydraulic jump and the backwash ripples. Some seaward return flow would continue even after the bore with its undular jump had become dissipated and disappeared. This caused the backwash ripples to begin to migrate down the beach face; the actual migration involves only a few centimeters, but it causes the characteristic asymmetrical shapes of the backwash ripples with the appearance of offshore migration (Figure 1). The backwash ripples are surprisingly stable; larger backwash ripples could still be clearly seen even after several waves passed over them.

The undular hydraulic jumps generally had six to ten wavelets, the average being eight. As will be seen, the number of backwash ripples formed by the jump would generally equal the number of wavelets.

The undular jump is only one type of hydraulic jump. In general, a hydraulic jump is a sudden transition from "supercritical" to "subcritical" flow. These flow regimes are defined in terms of the Froude Number

$$F = \frac{u}{\sqrt{gh}} \qquad (1)$$

where u is the dimensional water velocity, h is the local dimensional water depth, and g is the acceleration of gravity. The flow is respectively supercritical when $F > 1$ and subcritical when $F < 1$. The transition from supercritical to subcritical regimes can be accomplished by the flow going through a hydraulic jump, which occurs at the position where $F = 1$ ("critical" flow). The hydraulic jump can be thought

of as a wave form which moves upstream with a velocity $\sqrt{gh}$ which is equal to the downstream water flow u so that the wave form is stationary in position (since F = 1).

The type of hydraulic jump depends on the value of the Froude number before the jump occurs, that is, its value in the supercritical stage. The types recognized are outlined in Figure 3 together with the Froude number range; there is actually a continuum of types so the classification of Figure 3 is somewhat artifical. The true undular jump with its wavelets, important to the present study, is limited to Froude numbers less than 2. At higher Froude numbers the wavelets break. Such transitional jumps with breaking wavelets were at times observed on the beaches, but only very rarely. The fully turbulent jump has no wavelets and cannot therefore form backwash ripples.

Direct determinations of the Froude number of the backwash down the beach face are difficult to make because of the problem of measuring the flow velocity u in the very shallow but rapidly flowing water. Some measurements of the depth h were obtained and were found to be on the order of 10 cm. This depth implies a velocity of between 100-200 cm/sec for the correct Froude numbers for the occurrence of an undular hydraulic jump. These velocities are quite reasonable, supporting the idea of a true undular hydraulic jump forming by the collision of the backwash and an incoming wave bore.

In addition to the observations of undular hydraulic jumps on beaches, some measurements were made of the resulting backwash ripples.

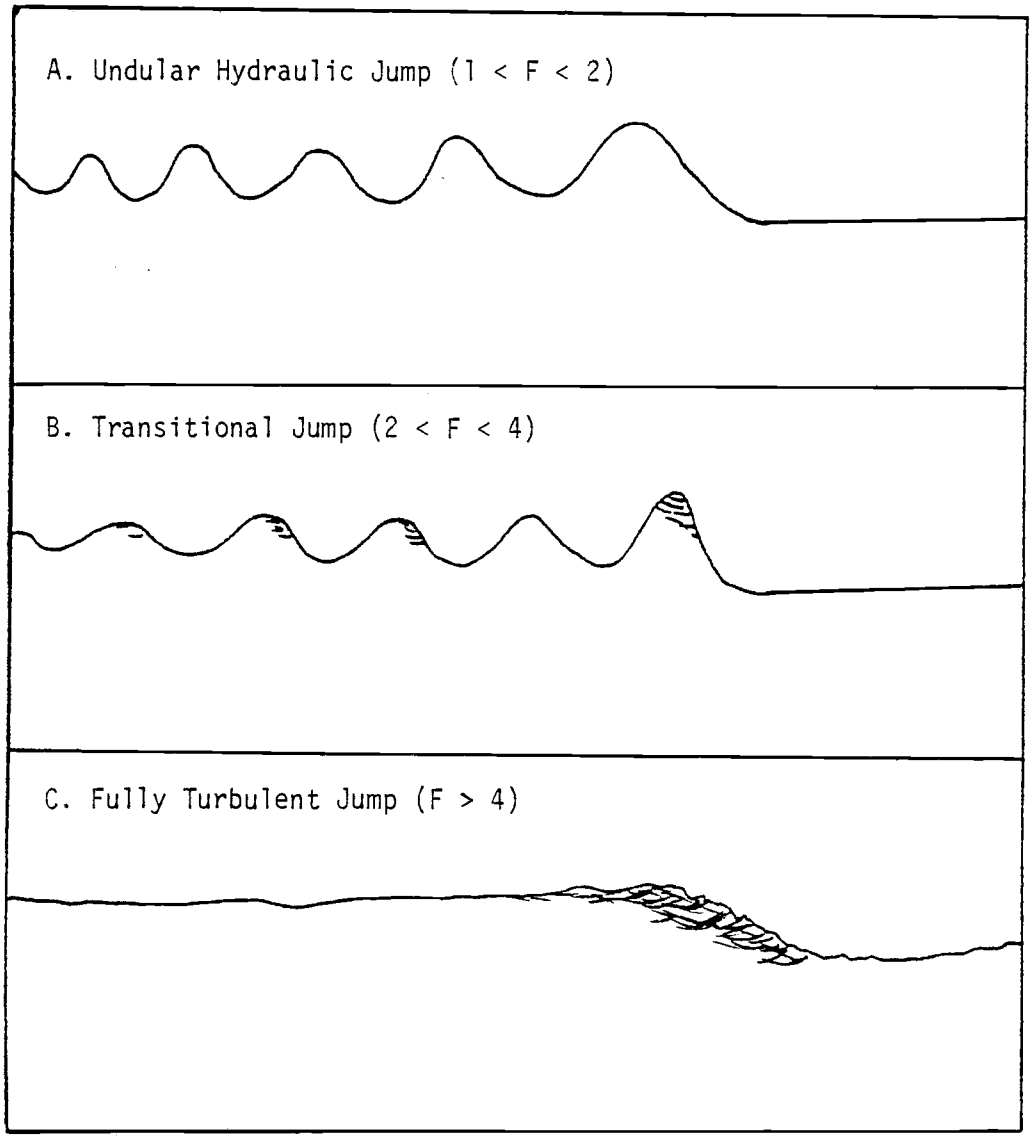

Figure 3: The three different kinds of hydraulic jumps on the basis of the Froude number $F = u/\sqrt{gh}$.

These were obtained at low tide using a 100-ft surveyor's tape stretched out across the exposed beach face. The positions of each successive ripple crest and trough were noted so that we could determine whether there are any offshore variations in ripple spacings. Measurements would be made by sets, the sets presumably formed under individual jumps. As can be seen in Figure 1, on Agate Beach there are so many ripples that it is difficult to tell where one set begins and another ends. On other beaches (for example, Figure 2), individual sets are more clearly identifiable, and there it is seen that a set usually comprises some six to ten ripples, the same number as water undulations in the jump, as is expected.

Table 1 gives the mean spacings of several sets of measured backwash ripples. It is seen that the mean spacings range from 48 to 70 cm. The spacings are higher than 20-50 cm spacings reported by Tanner (1965). This range of ripple spacings is produced by the range of size-scales of hydraulic jumps observed on the beaches; that is, there is actually a range of sizes of undular hydraulic jumps found. It should be realized that the nature of the hydraulic jump is governed by the Froude number of equation (1) which is a dimensionless number. Therefore, there can be different sizes of hydraulic jumps which will otherwise be the same so long as the initial Froude number in the supercritical region is the same. This was confirmed by observations on the beach of different size undular jumps which otherwise did have the same flow characteristics. The observed wavelet undulations

TABLE 1. - *Field measurements of backwash ripple spacings*

	Ave. Spacing $\bar{\lambda}$, cm	Number of Ripples	Standard Deviation
AGATE BEACH	70	10	2.3
	69	7	2.2
	59	6	3.1
	60	9	4.0
	60	7	3.7
	59	3	1.0
	53	5	1.0
	51	11	2.1
	58	5	
	69	7	
	54	7	
	67	10	
DEVIL'S PUNCHBOWL BEACH	48	4	
	50	3	

ranged approximately from 50 to 75 cm in the different jumps, the range of wavelengths which would be required to form the backwash ripple wavelengths given in Table 1.

Figure 4 gives the offshore variations of spacings within individual sets of backwash ripples. It is seen that there is a tendency for the wavelengths to decrease in the offshore direction, that is, with distance from the jump face. We will see in the next section that the mathematical simulation of an undular hydraulic jump displays similar offshore decreases in the wavelengths of the undulations. Due to difficulties of measurement, direct measurements of offshore variations in wavelengths of the wavelets in the field and laboratory jumps could not be made.

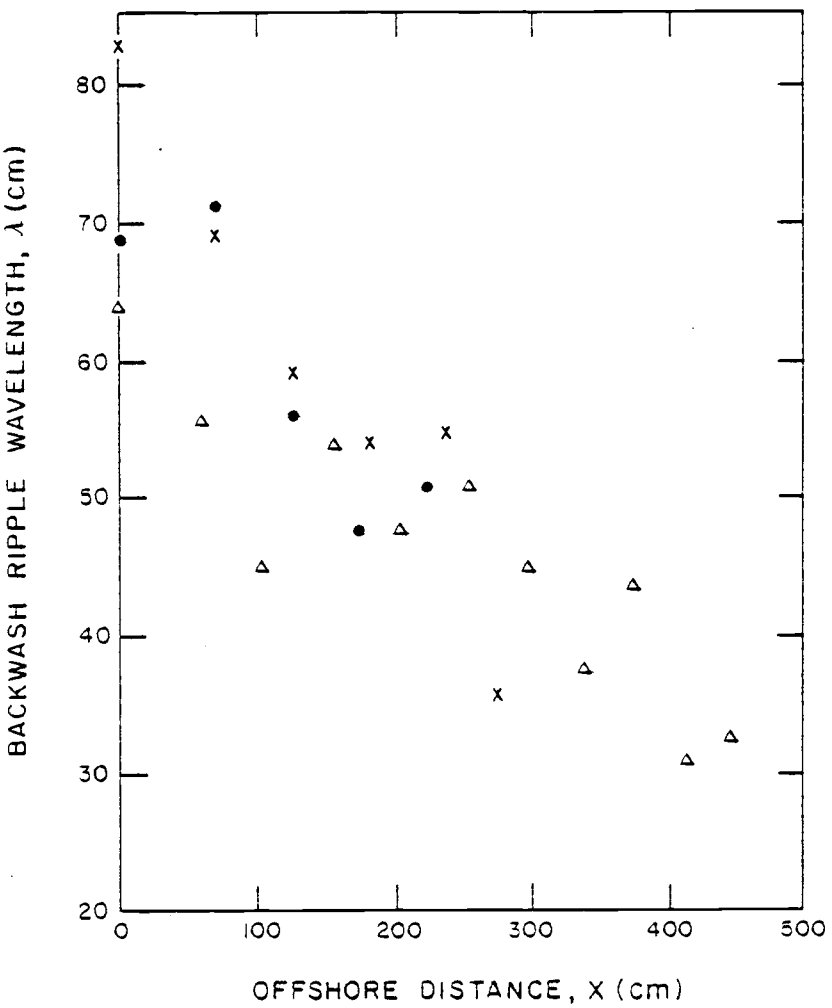

Figure 4: The offshore variations in backwash ripple wavelengths for three sets of ripples, each symbol representing a different group of ripples.

THE COMPUTER SIMULATION MODEL

Many of the properties of undular hydraulic jumps and the ripples they produced can be investigated by means of a model which simulates the water flow and the resulting patterns of sediment transport. The undular hydraulic jump itself may be described by a set of equations called the Boussinesq equations. In nondimensional form these equations are the continuity equation

$$\frac{\partial \eta}{\partial T} + \frac{\partial}{\partial X}\left[(\eta + 1)U'\right] = 0 \qquad (2)$$

and the momentum equation

$$\frac{\partial \eta}{\partial X} + \frac{\partial U'}{\partial T} + \varepsilon U' \frac{\partial U'}{\partial X} = \frac{1}{3}\mu \frac{\partial^3 U'}{\partial X^2 \partial T} + O(\varepsilon\mu, \mu^2) \qquad (3)$$

where η is the difference in water level from the reference height h (Figure 5), U' is the dimensionless mean horizontal particle velocity, ε is a small parameter equal to the wave amplitude divided by the depth h, and $\mu = h_o^2/\ell^2$ where h_o is a vertical scale and ℓ is a horizontal length scale to be determined later. The complete derivation of these equations can be found in Appendix I. The continuity equation (2) basically keeps track of the total quantity of water, insuring that no water will be created nor destroyed in the flow. The momentum equation (3) balances the forces acting on the flow.

The solutions of equation (2) and (3) together with the necessary boundary conditions yield the patterns of flow within the undular

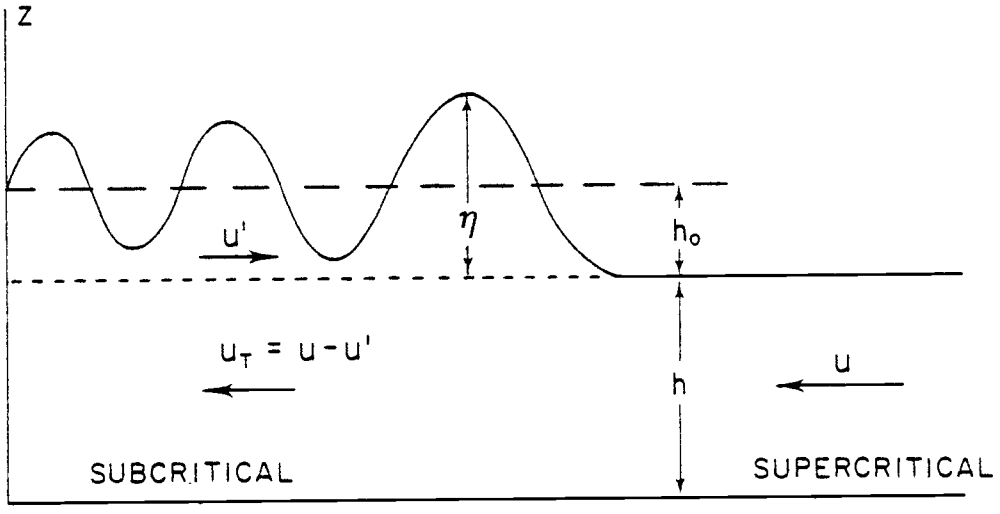

Figure 5: A diagram of the different symbols used in the text. The supercritical flow is from right to left, the particle speed is left to right and the resulting mean flow in the subcritical region is from right to left.

hydraulic jump. The necessary numerical work is discussed in Appendix II (Peregrine, 1966). In order to actually solve the equations with the specified initial conditions, we must specify several parameters. For equations as non-linear as equation (3) we must choose the mesh sizes (Δx and Δt) by trial and error. To achieve stable results the mesh ratio $\Delta t/\Delta x$ is reduced until the results are independent of the mesh sizes. The initial conditions are chosen to give a reasonable surface profile that is not too abrupt for the model to handle. Testing has shown that an initial amplitude $\eta_0 = 0.1$ is a good choice. The only remaining parameters in equation (3) are ε and μ. An examination of the experimental data to be presented later (Figure 9) reveals that the ratio of wave amplitude to water depth is about 0.4; this fixes $\varepsilon = 0.4$. Our basic problem with finding a value for μ is that our one-dimensional model has no imposed horizontal or vertical length scales. This leaves ℓ and thus μ as free parameters in the model. The only restriction imposed on μ is that it must be less than one. One of the goals of the comparison between the numerical model and undular hydraulic jumps generated in a laboratory flume is to determine how ℓ and μ are to be selected.

The second half of the model describes the backwash ripples by considering the continuity equation for sand. The one-dimensional continuity equation is

$$\frac{\partial C}{\partial t} = - \frac{\partial C u_T}{\partial x} \qquad (4)$$

where C is the concentration of sand and is a function of time only. The quantity Cu_T on the right side of equation (4) is the volume flux of sand; it is represented by q_s. The right side of equation (4) is the divergence of the volume flux. The divergence of the volume flux is equal to the difference in volume flux through the two vertical sides of the unit volume. This difference is simply equal to the time rate of change of the sediment interface height in the unit volume

$$\frac{\partial z}{\partial t} = - \frac{\partial q_s}{\partial x} \tag{5}$$

where z is the interface height and is related to the concentration of sand in a unit volume.

There are, of course, many equations that have been proposed to predict sediment transport rates for given water flows. One of the easier to employ, especially in the present application, is that of Chang et al. (1967) which has the form

$$W_s = K_T \bar{u}_T [\tau - \tau_c] \tag{6}$$

where W_s is the weight flux of sediment, K_T is an empirical constant, $\bar{u}_T$ is the total mean horizontal water velocity, τ is the stress exerted on the bottom by the water flow, and τ_c is the critical stress required to initiate sediment motion. W_s of equation (6) is the weight flux of sand transport; the volume flux q_s is given by

$$q_s = \frac{W_s}{g\rho_s} = \frac{K_T}{g\rho_s} \bar{u}_T [\tau - \tau_c] \tag{7}$$

where ρ_s is the density of the sand grains.

Next we must relate the bottom shear stress τ of the flow to the velocity. The well accepted method is to use the "drag law" relationship

$$\tau = C_f \rho \bar{u}_T^2 \tag{8}$$

where C_f is an empirical drag coefficient and ρ is the density of water. C_f can be obtained from a Moody diagram [for example, from Hansen (1969, Figure 11.2) where $C_f = f/8$]. In the models developed here, we used $C_f = 0.005$ which is a reasonable value for the jumps observed on the beaches.

The value of the empirical K_T in equation (7) is obtained from curves provided by Chang et al. (1967). The critical threshold stress τ_c is provided by the curves summarized in Miller et al. (1977) based on many sets of data. Equations (7) and (8) are combined to give an equation relating the volume flux of sand to the fluid velocity

$$q_s = \frac{K_T}{\rho g} \bar{u}_T [C_f \rho \bar{u}_T^2 - \tau_c] \tag{10}$$

Equation (10) is then substituted into equation (5) giving

$$\frac{\partial z}{\partial t} = - \frac{K_T}{\rho_s g} \frac{\partial \bar{u}_T}{\partial x} [3 C_f \rho \bar{u}_T^2 - \tau_c] \tag{11}$$

Equation (11) shows that the erosion or deposition of the sediment interface with time depends on the quantity $\bar{u}_T^2 \frac{\partial \bar{u}_T}{\partial x}$. Therefore, the phase relation between the velocity and the sediment interface is no

longer straightforward and numerical methods should be used to investigate the relationships.

Figure 6 shows an example of the results of the computer model. In this example, the sand was assumed to be quartz (ρ_s = 2.65 g/cm^3) with a mean diameter of 0.05 cm; a value which corresponds to the beaches in the study. This gives K_T = 0.4 from Chang et al. (1967), and τ_c = 2.25 dynes/dm^2 from Miller et al. (1977). The model was run with μ= 0.8.

Figure 6 shows a detailed time-history of the development of the undular hydraulic jump and formation of ripples in the sand. The times T for the stages of development are dimensionless times; the characteristic time required to convert to dimensional units will be found shortly.

Several things may be noticed about the computer model results in Figure 6. At large times many small wavelets have formed a large distance from the face of the jump; friction and surface tension would tend to damp these small wavelets out in practice. In the field observations the amplitude of the wavelets and the resulting backwash ripples decreased away from the face of the jump (see Figure 2). This same result may be noticed in the computer model. The affects of friction and surface tension would serve to reinforce this tendency and make the model even more realistic. Finally it should be noted that the model runs for longer than an undular hydraulic jump would physically be expected to last. For a typical field measurement of

Figure 6: The results of the computer model with $\mu = 0.8$, $\Delta X = 1.0$, $\Delta T = 0.5$ and the total horizontal length is 240 nondimensional units. Shown are the water surface profile, η , the horizontal velocity, U, and the profile of the backwash ripples, Z (highly vertically exaggerated). All are given in nondimensional terms.

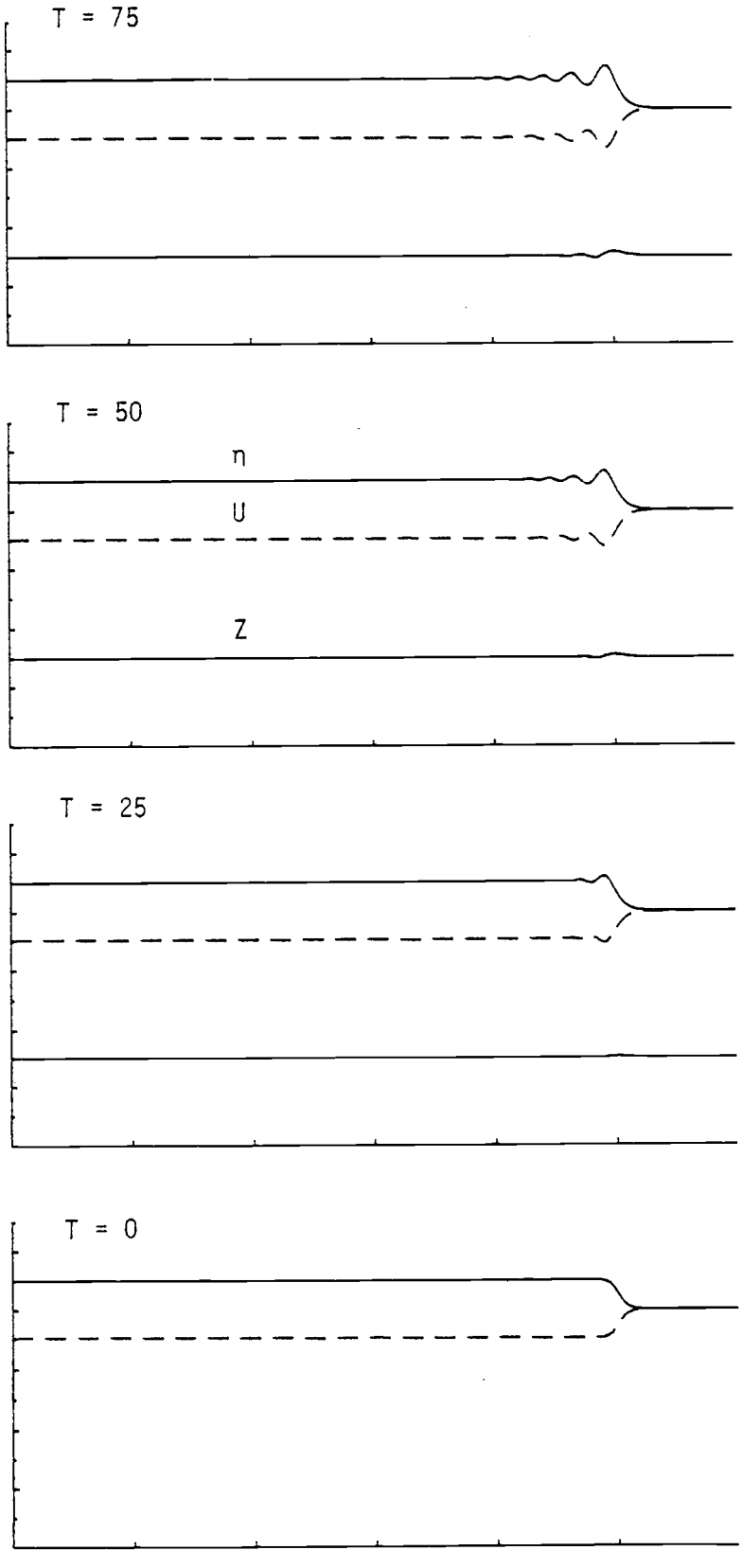
T = 75
T = 50
η
U
Z
T = 25
T = 0

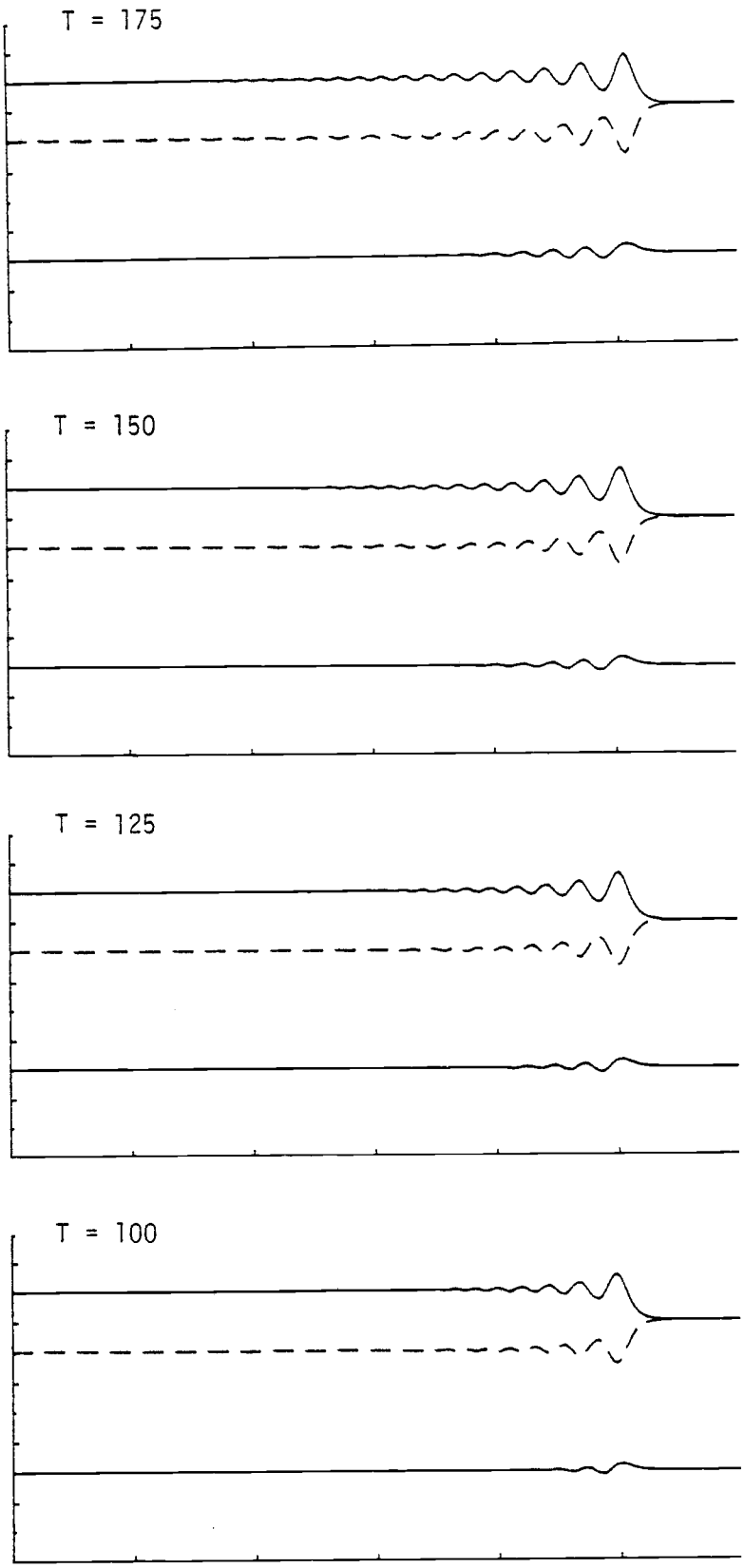
T = 175
T = 150
T = 125
T = 100

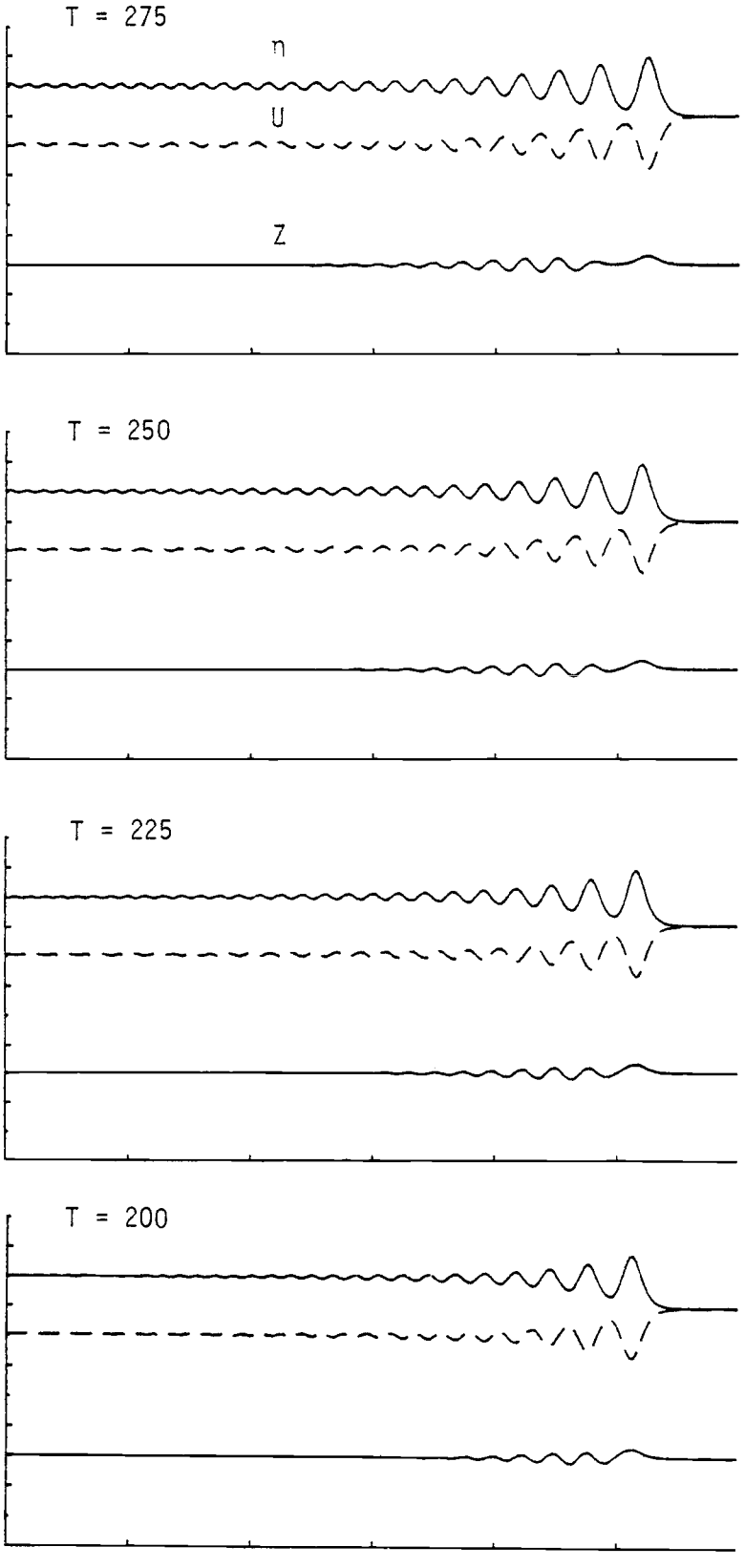
T = 275
η
U
Z
T = 250
T = 225
T = 200

$\bar{\lambda}$ = 60 cm and h_o assumed to be 5 cm, T = 200 is the maximum time one would expect the jump to last.

An expanded view of the undular hydraulic jump and the resulting backwash ripples is shown in Figure 7 and a variable phase shift between the surface profile and bed profile is apparent. As mentioned before this variable phase shift is due to the fact that changes in the bed profile depend on the quantity $\bar{u}_T^2 \frac{\partial \bar{u}_T}{\partial x}$; this quantity is proportioned to $\frac{\partial q_s}{\partial x}$ in Figure 7. From Figure 7 and Equation 10 it can be seen that q_s is in phase with u_T. As expected $\frac{\partial q_s}{\partial x}$ is not in phase with either u_T^2 or $\frac{\partial u_T}{\partial x}$. However, the difference in phase between $\frac{\partial q_s}{\partial x}$ and u_T^2 or $\frac{\partial u_T}{\partial x}$ are small compared with the phase shift between $\frac{\partial q_s}{\partial x}$ and z. Equation 5 states that $\frac{\partial q_s}{\partial x}$ and $\frac{\partial z}{\partial t}$ must be in phase. From this we conclude that the major portion of the observed phase shift between z and n is due to the time dependent nature of the flow. These results are not expected to be observable in the field. Even if both the hydraulic jump and the resulting backwash ripples could be measured together the phase shifts are so small that they would be masked by measurement error and the shift of the ripple sets due to swash that flowed over the ripples after the hydraulic jump died out.

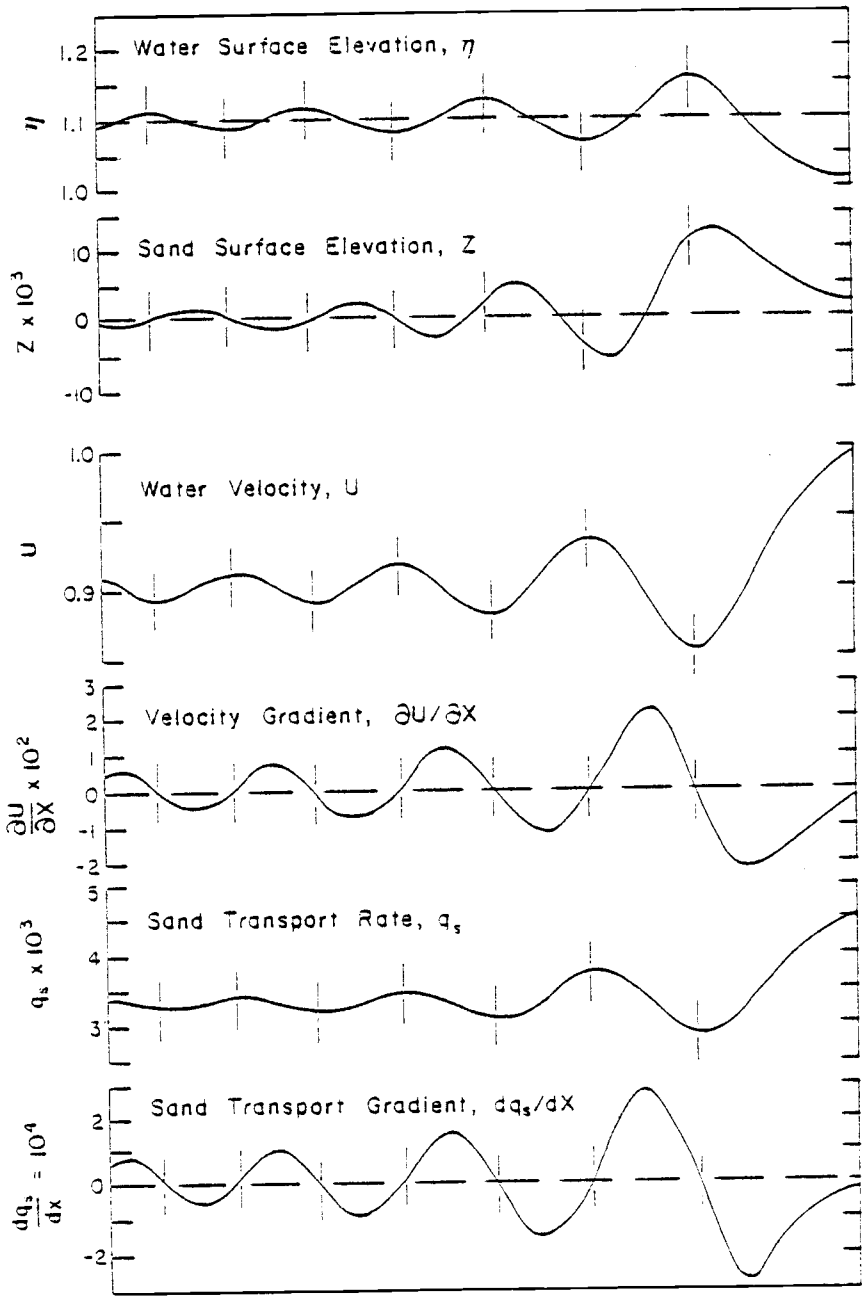

Figure 7: An expanded view of the undular hydraulic jump showing the phase lag difference between the surface and bed profiles. Note that the third and fourth ripples from the face are in phase while the leading two ripples are out of phase. Also shown are the water velocities, the sediment transport and the gradients in the transport. See text for detailed discussion.

DETERMINATION OF THE HORIZONTAL LENGTH SCALE ℓ

With the computer model different sets of parameters (such as μ) model different experimental conditions. Because of this we need to decide what values of the parameters are appropriate for the computer model to most closely approximate the field conditions. Given a measured h_o, we need the horizontal length scale ℓ for a particular field observation in order to calculate μ for that experiment. Given the μ we then calculate the computer results that most closely approximate the field condition; we will then use the length scale ℓ to transform the results to dimensional form for direct comparison.

The results of the computer model with arbitrary μ are shown in Figure 8, the nondimensional mean wavelength ($\bar{\lambda}/\ell$) versus μ. We chose to use the mean wavelength in order to include the effects of a variation of λ with distance away from the face of the jump, and in order to keep the same range of measurement in as the experimental results we consistently measured the first six wavelengths for the calculation of the mean. We found that the undular hydraulic jump grows more slowly with decreasing μ and we had to be careful to wait until the jump reached the same "maturity" in each case before calculating a $\bar{\lambda}/\ell$. Figure 8 shows a strong linear dependence and we chose this dependence between $\bar{\lambda}/\ell$ and μ for our calculations.

Solve the following empirical equation for ℓ

$$\frac{\bar{\lambda}}{\ell} = m \frac{h_o^2}{\ell^2} + b \qquad (12)$$

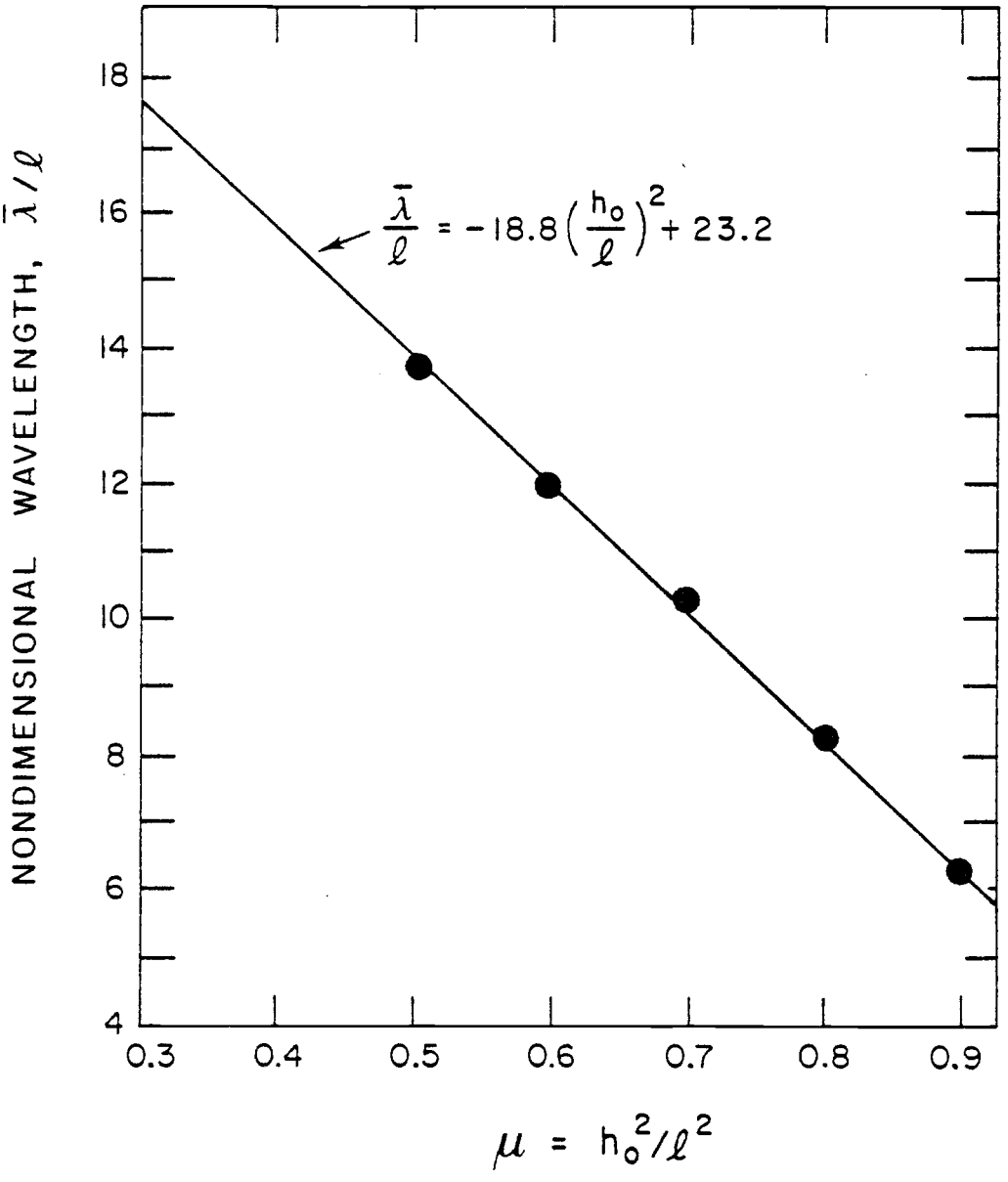

Figure 8: The variation in mean wavelength ($\bar{\lambda}$ defined as the mean of the first six wavelengths) with μ. The linear dependence of $\bar{\lambda}$ on μ demonstrates a relationship between the parameters of the computer model and measured quantities in the field.

where m = -18.8 is the slope and b = 23.2 the intercept of the linear regression in Figure 8. The result is

$$\ell = \frac{1}{2b} \left(\bar{\lambda} + \sqrt{\bar{\lambda}^2 - 4mbh_o^2} \right) \tag{13}$$

This result gives us ℓ as a function of the dimensional wavelength and depth scale for any particular experimental condition. Note that we have now specified μ and used one equation to solve for only one unknown ℓ.

No vertical length scale is imposed by the conditions of the jump because in principal a given hydraulic jump may form with any supercritical depth h. Therefore, we must seek the vertical scale in the undular hydraulic jump itself. We chose to use the average vertical rise in water depth from the supercritical to the subcritical region of the hydraulic jump. This h_o is shown in Figure 5. Using Equation 13 and h_o we may find μ for a particular set of experimental conditions and, therefore, calculate the model results most appropriate for that particular experiment. We then use the result of Equation 13 to scale the model. In particular, we can use this technique to investigate the time history of the backwash ripples reported in the field section of this work.

If we choose as an example a $\bar{\lambda}$ of 60 cm from Table I and assume a vertical scale of 5 cm; from Equation 13 we find that ℓ = 5.8 cm and, therefore, μ = 0.75. The results presented in Figure 6 have a μ = .8 and so by simply multiplying the horizontal scale by 5.8 cm we have a

dimensional time history of the backwash ripples measured in the field. The characteristic time for this example is 0.08 sec. If the nondomensional time T is multiplied by this factor, the result is the dimensional time t. Of course, the vertical axis must be multiplied by h_o to dimensionalize the vertical scale. However, the backwash ripple in Figure 7 have been vertically exaggerated for clarity and so are unrealistically high. The horizontal scale is the measured parameter in any event. It should be noted, however, that at best these are only approximate calculations. For instance, calculation of ℓ for the experimental results show an approximately 20 percent error if this ℓ is used to scale the first wavelength of the computer model. Considering the theoretical and practical assumptions used in these calculations that error is probably as small as we could expect.

As a further check on the computer model results, consider Figure 10. This is a plot of the dimensionless wavelength against the dimensionless distance from the face of the jump. Since both the wavelength and the horizontal distance are scaled with ℓ we may compare Figure 10 to the field measurements in Figure 5. The slopes of the two plots are virtually teh same. The field measurements fall off with a slope of -.116 and the computer model results in Figure 10 fall off with a slope of -.111. The good agreement, while not conclusive, is encouraging and supports the validity of the model.

LABORATORY EXPERIMENTS

Due to the difficulty of making careful observations and measurements on the undular hydraulic jumps occurring on the beaches, it was decided to undertake a series of laboratory experiments in which jumps are generated in a flume. The purpose of these observations is to provide data from real undular jumps which can be compared with the computer simulation model and used to calibrate the computer model's scale.

The experiments were performed in a 0.5 m wide by 7.3 m long flume at Oregon State University. The flume was tilted to a slope of 0.005, and water at a flow rate of 0.35 $\pm$ 0.05 cfs was introduced at the high end. The downstream depth was controlled by a gate at the exit end of the flume; by small variations of this downstream depth the position of the jump could be controlled. The upstream conditions were dependent upon the flow-rate and the flume slope. The formation of an undular hydraulic jump required that the Froude number [equation (1)] be greater than unity but less than approximately two. After the undular jump reached stability the surface heights of the undulations were measured with a vernier measuring rod with an accuracy of $\pm$ 0.15 cm. The mean horizontal velocities were measured with a pitot tube and water manometer with an accuracy of $\pm$ 5.0 cm/sec.

The experiments were originally intended to have a sand bottom so that direct observations could be made of the sediment transport patterns leading to the formation of the ripples. However, the velocities

in the supercritical region are so high that unless a continuous supply of sand is added to the flume the bottom quickly erodes away. In addition, the large changes in bottom topography soon destroyed the conditions required for the formation of an undular jump. That is, both the velocity u and the depth h in the supercritical region changed with time in such a way as to lower the Froude number and to thus eliminate the jump. If such experiments are to be performed, they must duplicate more closely the natural conditions found on the beach where there is a continuous supply of sand. This could be done either by having an initially large supply of sand in the flume or by utilizing a recirculating sand flume; neither option was unfortunately available to us in these experiments.

The measurements of the hydraulic jump itself also presented problems. The position of the jump is a delicate balance of a nonlinear upstream velocity and a mean downstream velocity. This balance was constantly making small changes in the position of the jump as small perturbations changed each velocity. As a result it was difficult to make measurements of velocities and heights of the undulations with respect to a fixed point. However, by measuring all values with respect to the first peak ($x = 0$ at the first peak) this problem was largely avoided.

The experimental results are shown in Figure 9 for Froude numbers 1.4, 1.6 and 1.9. All show the surface wavelets or undulations typical of the undular hydraulic jump. The undulations continued for the entire length of the flume; however, only the first five or six were sufficiently

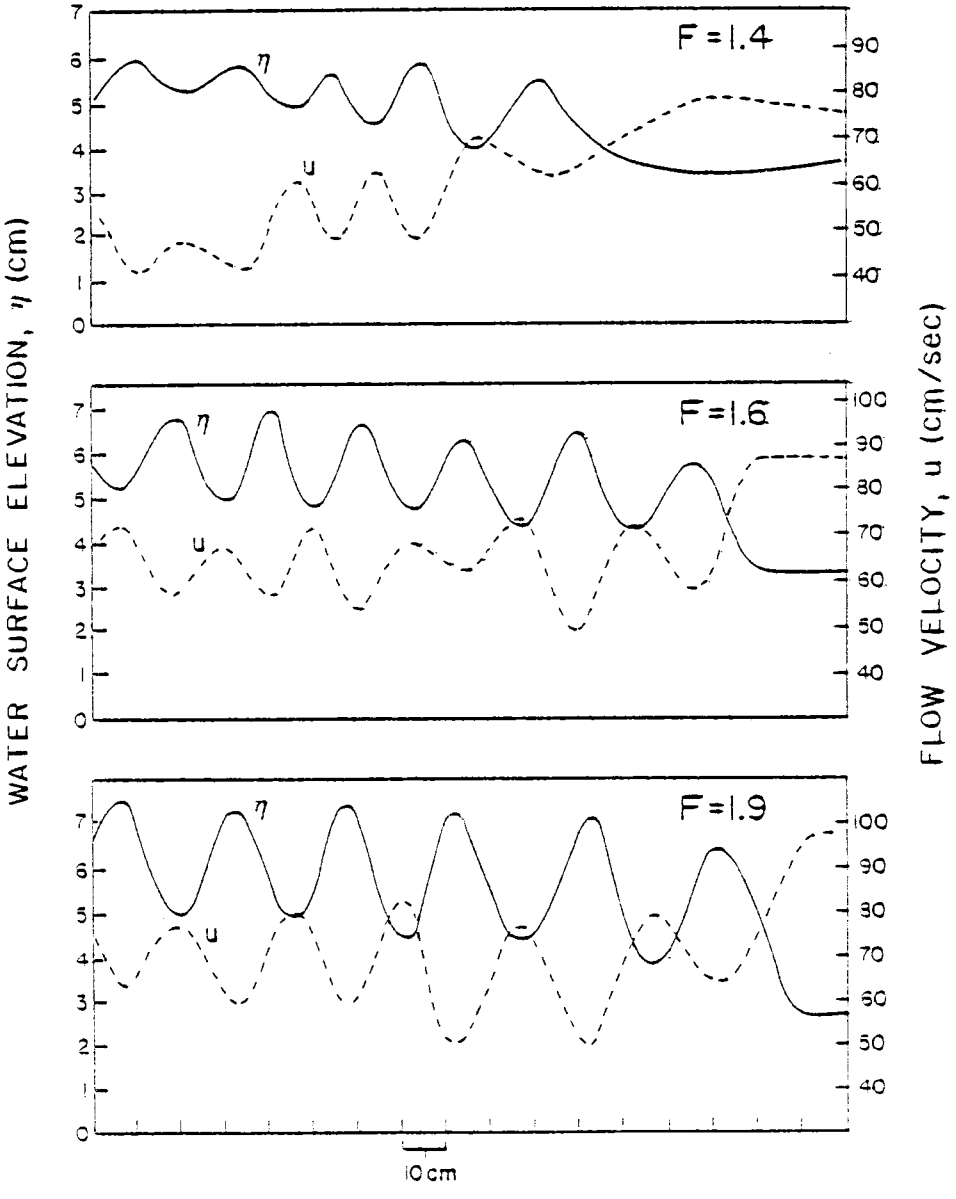

Figure 9: Experimental results of undular hydraulic jumps in a laboratory flume covering the range of interest for this study.

well-developed to make accurate measurements. All measurements were made after the jumps had essentially reached steady-state. For this reason, the laboratory observations should correspond to large dimensionless times T in the computer models (Figure 6). The velocities recorded in Figure 9 are at mid-depth (half way from the water surface to the bottom) at each position. Due to bottom drag the velocity of course decreases to zero at the bottom so that there is a continuous vertical variation in the velocity as well. But as seen in Figure 10, a measured of the velocity at mid-depth is a reasonable estimate of the average flow velocity.

If the laboratory results (Figure 9) and the computer simulation results (Figure 6) are compared, it is seen that there is a close similarity of overall appearance. In the experimental results the tops of the undulations are progressively higher in the direction of flow such that the top of the first wavelet tends to be lower than the second, and so on. This is opposite to the simulation results (Figure 6) where the top of the first wavelet is the highest because it has the greatest amplitude. This results from the non-inclusion of boundary drag in the simulation model which is of course present in the laboratory results. The effect of the bottom drag is to increase the overall water depth of the flow downstream from the face of the jump. Thus the undulations in the laboratory jumps are superimposed upon a progressive increase in water depth in the direction of flow having the effect of raising the levels of successive crests of the undulations. The jump

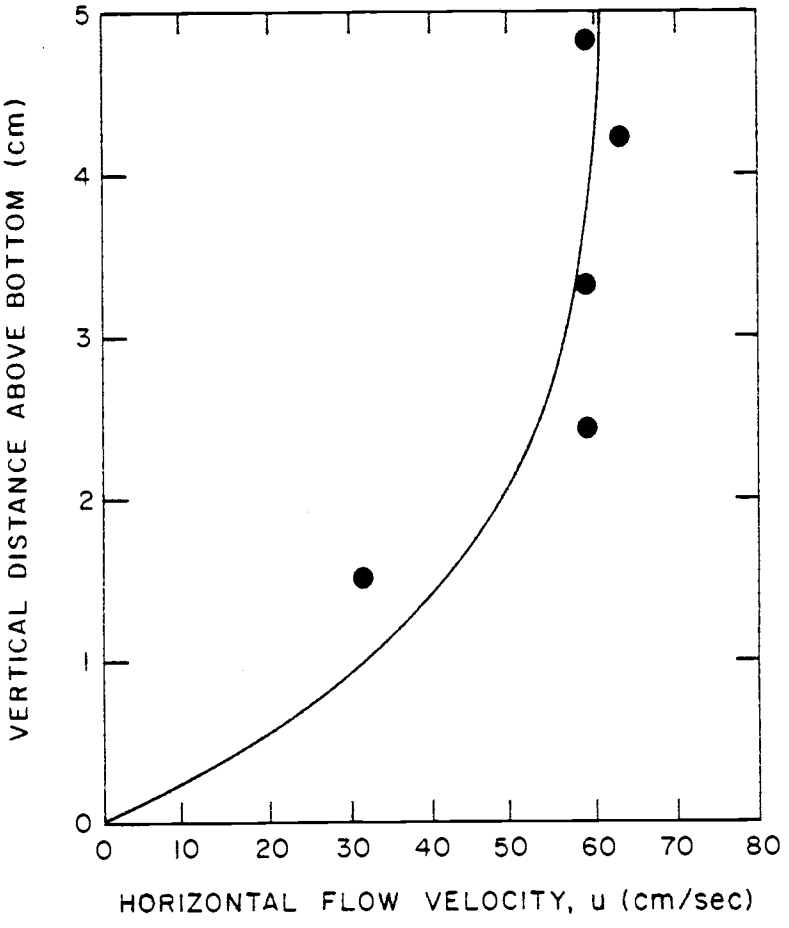

Figure 10: The horizontal velocity at different depths beneath the first peak of a jump with a Froude number equal to 1.7. The center velocity is a good approximation of the mean velocity of the flow.

at Fr = 1.4 of Figure 9 shows the closest similarity to those observed on the beaches and to the simulation models (Figure 6) with respect to the first undulation being the largest and to there being a decrease in the wavelengths of the undulations away from the front of the jump. The jumps at Fr = 1.6 and 1.9 do show a small tendency to have decreasing undulation wavelengths away from the jump front, but the changes are small and approach the uncertainties in the measurements. At these higher Froude numbers there is little apparent decrease in the amplitudes of the wavelets with distance from the jump front, unlike the laboratory results at Fr = 1.4 (Figure 9), those observed on beaches, and the jumps produced by the computer simulation at low Froude numbers. According to the laboratory results of Figure 9, there is a small increase in the wavelengths with increasing Froude number, the average wavelengths going from 23 to 25 to 27 cm as the Froude number is increased. Thus, there would appear to be relatively little dependence of the spacings of the resulting ripples on the Froude number. More important would be the scale of the experiment; as discussed earlier, a larger-scale experiment would produce larger wavelets and backwash ripples even though the Froude numbers of the large- and small-scale experiments are the same.

CONCLUSIONS

The goal of this work is to explore the details of sediment transport under an undular jump. The experiments have validated the computer model. The model shows the development of ripples in the sand and shows their relatively fast time scales and their close adherence to the form of the undulations in the water. Interestingly, good qualitative agreement was found even though there was no feedback mechanism from the sediment to the water. That is, the sand ripples do not seem to affect the undulations. This is in contrast to dunes and antidunes whose ripple index is small enough that there is significant feedback from the sediment to the water (Kennedy, 1963). The time required for the model to reach approximately steady-state, about ten dimensional seconds, agrees with experimental and field observations. This time is about what is available in the upper swash zone before another wave enters the zone and destroys the jump.

Finally, the most gratifying result from the study is the relative unimportance of friction in the water. This has been shown by other workers (Hawaleska et al., 1970). Note that this does not mean friction is unimportant at the boundary. It does mean that internal viscous and turbulent dissipation is unimportant in the water itself over the time and length scales found. This is in accordance with theoretical predictions (Meyer, 1967). Friction is of course required to couple the water to the sand.

The use of numerical modeling of high energy environments is both

possible and necessary. In such a region even laboratory experiments become difficult and analytic theory beocmes impossible. This study has shown the utility of modeling to provide details of high energy boundary regions that would be difficult or impossible to find by other means. It has also shown the importance of careful interpretation of modeling results using appropriate experimental data for comparison. This point should be emphasized. The model itself provides little insight about the flow. Only when the model is critically compared to experiments do appropriate scales emerge.

The results of this model may be used in many different environments such as river mouths and spillways. Given a mean wavelength and a depth scale from field measurements the formation of the resulting sand ripples may be studied. Measurements of the persistence of the jump could give an understanding of the amount of sediment transport in both the subcritical and supercritical regions. It is also obvious that predictions of sediment transport and flow velocities are not possible from the measurement of the wavelength unless a depth scale is known as well. This is unfortunate since many times the wavelength is all that is measured and the parameters of the flow regime is what is of interest. The existence of such waveforms does place limits on the flow parameters since no waves would form if the Froude number is greater than two or less than one.

REFERENCES CITED

Batchelor, G.K., 1967, An introduction to Fluid Dynamics: Cambridge University Press, Cambridge, Chapter 3.

Bennett, A.F., 1976, Open boundary conditions for dispersive waves: Journal of the Atmospheric Sciences, v. 33, p. 176-182.

Boussinesq, J., 1872, Liouvilles J. Math., v. 17, 55 p.

Broer, L.J.F., 1964. On the interaction of non-linearity and dispersion in wave propagation: Applied Science Research, section B, v. 11, p. 273-285.

Chang, F.-M., D.B. Simons, and E.V. Richardson, 1967, Total bedmaterial discharge in alluvial channels: Intern. Assoc. Hydr. Res., 12th Congress, Fort Collins.

Chen, J.H., 1973, Numerical boundary conditions and computational modes: Jour. of Comp. Physics, v. 13, p. 522-535.

Hanson, A.G., 1967, Fluid Mechanics: John Wiley and Sons, New York, 531 p.

Hayes, M.O., 1972, Forms of sediment accumulation in the beach zone: In Waves on Beaches, (R.E. Meyer, ed.), Academic Press, New York, p. 297-356.

Hawaleshka, O., and S.G. Savage, 1970, The development of undular bores with friction: Proceed. of the 12th Coastal Engineering Conf., Washington, D.C.

Kennedy, J.F., 1963. The mechanics of dunes and antidunes in erodible bed channels: Jour. of Fluid Mech., v. 16, pt. 4, p. 521-544.

Komar, P.D., 1976, Beach Processes and Sedimentation: Prentice-Hall, Inc., 429 p.

Lamb, H., 1932, Hydrodynamics: Dover Publications, New York, 787 p.

Meyer, R.E., 1967, Note on the Undular Jump: Jour. Fluid Mech., v. 28, pt. 2, p. 209-221.

Miller, M.C., I.N. McCave, and P.D. Komar, 1977, Threshold of sediment motion under unidirectional currents: Sedimentology, v. 24, p. 507-527.

Miller, R.L., 1968, Experimental determination of run-up of undular and fully developed bores: Jour. of Geoph. Res., v. 73, n. 14, p. 4497-4510.

Peregrine, D.H., 1966, Calculations of the development of an undular bore: Jour. of Fluid, Mech., v. 25, p. 321-330.

Tanner, W.F., 1965, High-index ripple marks in the swash zone. J. Sediment. Petrol., v. 35, p. 968.

Witham, G.B., 1974, Linear and Non-Linear Waves: Series on Pure and Applied Mathematics: John Viley and Sons, New York, Chapt. 13.

APPENDIX I

Theory of an Undular Hydraulic Jump

As a first step in modeling the sediment profile a forcing function must be determined. Accepting rather restrictive assumptions, this has been done by several previous workers. The first derivation of the appropriate equations was by Boussinesq (1872). A considerably more recent and concise derivation is given in Whitham (1974). The derivation will give the Boussinesq Equations of nonlinear fluid flow.

We first start with the Navier-Stokes equations of fluid motion and apply the following set of assumptions; the fluid density is constant, the flow is irrotational and two-dimensional, the bottom boundary is impermeable, and the fluid is inviscid. The major assumption here is irrotationality; from this the equally unrealistic inviscid assumption follows. A moments thought will demonstrate how unrealistic this assumption must be in the flow regime we are considering. However, in order to make any progress at all we must make this assumption and it is gratifying how well the result compares to experimental measurements. The first equation we deal with is the equation of continuity

$$\frac{D\rho}{Dt} + \nabla \cdot \rho\vec{u}' = 0$$

where $\frac{D\rho}{Dt}$ = the material derivative,

ρ = the fluid density,

$\vec{u}'$ = horizontal particle velocity.

Lower case letters refer to dimensional quantities, upper case letters will refer to dimensionless quantities and primed velocities will be particle (or orbital) velocities. Figure 5 in the text diagrams these definitions.

Applying the assumptions given above to the continuity equation we have

$$\frac{\partial u'}{\partial x} + \frac{\partial w'}{\partial z} = 0$$

where w' = vertical particle velocity

x = horizontal coordinate

z = vertical coordinate (positive upward)

Vertically integrate through the water column from zero to the surface at $\eta + h$ and using the assumption of an impermeable bottom yields

$$\frac{d\eta}{dt} \int_0^{\eta + h} u'dz - u'(h + \eta) \frac{d\eta}{dx} + w'(\eta + h) = 0 \qquad \text{(A2)}$$

The kinematic boundary condition that particles on the surface remain there gives

$$w'(\eta + h) = \frac{d\eta}{dt} = \frac{\partial \eta}{\partial t} + u'(\eta + h) \frac{\partial \eta}{\partial x} \qquad \text{(A3)}$$

Apply this to equation (A2) and define a mean horizontal particle velocity $\bar{u}'$ as

$$u' = \frac{1}{\eta + h} \int_0^{\eta + h} u'dz$$

we find that

$$\frac{\partial \eta}{\partial t} + \frac{\eta}{\partial x}\left[\bar{u}'(\eta + h)\right] = 0$$

Nondimensionalize the above equation with the following characteristic terms

$$\begin{aligned} u' &= (gh_o)^{1/2} U' & x &= \ell X \\ t &= \ell(gh_o)^{-1/2} T & \eta_{dim} &= h_o \eta \end{aligned} \tag{A4}$$

where the upper case variables are dimensionless variables. The horizontal length scale is ℓ. The result is

$$\frac{\partial \eta}{\partial T} + \frac{\partial}{\partial X}\left[(\eta + 1)U'\right] = 0 \tag{A5}$$

This equation is the exact equation of continuity for the mean flow in an irrotational two-dimensional system where $\eta(x,t)$ is a deviation from a reference height h.

The second equation required for a complete description of the flow is the momentum equation. Applying the appropriate assumptions to the Navier-Stokes equations of conservation of momentum we have in three dimensions

$$\frac{\partial u'}{\partial t} + u' \cdot \nabla u' + \frac{1}{\rho} \nabla p + g\hat{k} = 0 \tag{A6}$$

(See G.K. Batchelor's Fluid Dynamics for a complete description of this equation.) Since the flow is irrotational and two dimensional we may

define a velocity potential

$$\nabla\Phi = \vec{u}' \tag{A7}$$

Combining equation (A6) and equation (A7) and integrating with respect to X we have a Bernoulli energy equation

$$\frac{\partial\Phi}{\partial t} + \frac{1}{2}\left[\left(\frac{\partial\Phi}{\partial x}\right)^2 + \left(\frac{\partial\Phi}{\partial z}\right)^2\right] + \frac{\rho}{\rho_o} + gz = M(t) \tag{A8}$$

where M(t) is an arbitrary function of time. We wish to solve equation (A8) at the surface $Z = h + \eta$ where the pressure is continuous, equal to the air pressure and defined to be zero. To do this we must nondimensionalize equation (A8) using the following characteristic terms

$$\begin{aligned} x_{dim} &= \ell x & h_{dim} + \eta_{dim} &= h_o(1 + \varepsilon\eta) \\ z_{dim} &= h_o z & t_{dim} &= \ell(gh_o)^{-1/2}T \\ & & \Phi_{dim} &= \varepsilon\ell(gh_o)^{1/2}\Phi \end{aligned} \tag{A9}$$

(see Broer, 1964). Where the subscript dim denotes dimensional variables in this case, ε is a small parameter to be determined and the characteristic of Φ comes from equation (A7). The introduction of ε is consistent with the earlier statement that η is of order h_o because ε is less than but of order one. A description of these parameters and somewhat different derivation than given here may be found in Broer (1964). Applying equations (A9) to (A8) we have

$$\varepsilon\eta + \varepsilon\frac{\partial\Phi}{\partial T} + \frac{\Phi^2}{2}\left[\left(\frac{\partial\Phi}{\partial X}\right)^2 + \frac{\ell^2}{h_o^2}\left(\frac{\partial\Phi}{\partial Z}\right)^2\right] = \frac{M(t)}{gh_o} - 1 \qquad \text{(A10)}$$

$M(t)$ is arbitrary and we can set $M(t) = gh_o$. Therefore, equation (A10) becomes

$$\eta + \frac{\partial\Phi}{\partial T} + \frac{\varepsilon}{2}\left[\left(\frac{\partial\Phi}{\partial X}\right)^2 + \frac{\ell^2}{h_o^2}\left(\frac{\partial\Phi}{\partial Z}\right)^2\right] = 0 \qquad \text{(A11)}$$

Now we wish to form equation (A11) in terms of only time and one space variable. Expand Φ in terms of a Taylor series expansion about 0,

$$\Phi(x,z,t) = \phi(x,t) + z\frac{\partial\phi(x,t)}{\partial z} + \frac{z^2}{2!}\frac{\partial^2\phi(x,t)}{\partial z^2} + \frac{z^3}{3!}\frac{\partial\phi(x,t)}{\partial z^3} + \frac{z^4}{4!}\frac{\partial^4\phi(x,t)}{\partial z^4} + \ldots \qquad \text{(a12)}$$

The velocity potential form of the continuity equation is Laplace's equation. Assuming an impermeable bottom at $Z = 0$

$$\frac{\partial\Phi}{\partial z} = 0 \qquad \text{(A13)}$$

From this and Laplace's equation we note that odd derivatives of Φ are zero. We assume no singularities between the bottom and the surface. Therefore, in the neighborhood defined by the bottom and the surface the Taylor series expansion of Φ is

$$\Phi(x,z,t) = \phi(x,t) - \frac{z^2}{2}\frac{\partial^2\phi}{\partial x^2} + \frac{z^4}{4!}\frac{\partial^4\phi}{\partial x^4} + \ldots \qquad \text{(A14)}$$

The terms in equations (A12) through (A14) are dimensional. If we non-dimensionalize equation (A14) by equations (A9)

$$\Phi = \phi - \frac{\mu Z^2}{2} \frac{\partial^2 \phi}{\partial X^2} + \frac{\mu^2 Z^4}{4!} \frac{\partial^4 \phi}{\partial X^4} + O(\mu^3) \tag{A15}$$

where $\mu = \frac{h_o^2}{\ell^2}$ and where ϕ does not depend on z. Now substitute equation (A15) into (A11) and keep terms of order ε and μ but dropping terms of order ε times μ and μ^2. Therefore, we have

$$\eta + \frac{\partial \phi}{\partial T} - \frac{\mu Z^2}{2} \frac{\partial^3 \phi}{\partial X^2 \partial T} + \frac{\varepsilon}{2} \left(\frac{\partial \phi}{\partial X}\right)^2 = 0 \tag{A16}$$

However, equations (A15) and (A11) were derived at the surface $Z = 1 + \varepsilon\eta$. Therefore, we have to the same order as equation (A16)

$$\eta + \frac{\partial \phi}{\partial T} + \frac{1}{2} \left(\frac{\partial \phi}{\partial X}\right)^2 = \frac{\mu}{2} \frac{\partial^3 \phi}{\partial X^2 \partial T} \tag{A17}$$

We are actually interested in an equation for the mean horizontal velocities. Consider the expansion of

$$\phi = \phi - \frac{Z^2 \mu}{2} \frac{\partial \phi}{\partial X^2} + O(\mu^2)$$

From equation (A7) and the definition of the mean velocity we have

$$U' = \frac{\partial \phi}{\partial X} - \frac{(1 + \varepsilon\eta)^2}{6} \frac{\partial^3 \phi}{\partial X^3} + O(\mu^2)$$

or

$$\frac{\partial \phi}{\partial X} = U' + 1/6\ \mu\ \frac{\partial^3 \phi}{\partial X^3} + O(\varepsilon^2, \mu^2) \qquad \text{(A18)}$$

Now consider equation (A17) once more. Take the partial derivative with respect to x of equation (A17). Substitute equation (A18) into the left side of the result, group terms and drop terms of order ε times μ and ε^2

$$\frac{\partial \eta}{\partial X} + \frac{\partial U'}{\partial T} + \varepsilon U' \frac{\partial U'}{\partial X} = 1/3\ \mu\ \frac{\partial^3 \frac{\partial \phi}{\partial X}}{\partial^2 X \partial T} \qquad \text{(A19)}$$

Substitute equation (A18) into the right hand side of equation (A19) gives

$$\frac{\partial \eta}{\partial X} + \frac{\partial U'}{\partial T} + \varepsilon U' \frac{\partial U'}{\partial X} = 1/3\ \mu\ \frac{\partial^3 U'}{\partial X^2 \partial T} + O(\varepsilon\mu, \mu^2) \qquad \text{(A20)}$$

We can recognize terms in equation (A20). $\frac{\partial \eta}{\partial X}$ is the gravity term, $\frac{\partial U'}{\partial T}$ is the time rate of change of mean velocity, $\varepsilon U' \frac{\partial U'}{\partial X}$ is the non-linear term and $\frac{\partial^3 U'}{\partial X^2 \partial T}$ is the dispersion term.

Equations (A5) and (A20) are sufficient to describe the motion of any shallow water wave with the effect of a small amount of dispersion included but with friction neglected. Those two equations are the Boussinesq equations and are a set of coupled non-linear partial differential equations that require one initial condition and two boundary conditions for their solutions. These conditions will describe the physical conditions required for an undular hydraulic jump to form.

Boundary Conditions

The boundary conditions are perhaps the simplest to imagine but cause the most trouble in the actual solution of the equations. Conceptually we want to form a step function in the water with $\eta=\eta_0$ for $x = -\infty$ and $\eta = 0$ for $x = \infty$ and $U' = 0$ for $x = -\infty$ and $x = \infty$. The initial condition at $T = 0$ is harder to visualize but is in fact easier to write in continuous form. Initially assume that dispersion may be neglected. We then have the shallow water wave equations and these may be solved exactly. Equations (A5) and (A20) without dispersion are

$$\frac{\partial U'}{\partial T} + \frac{\partial \eta}{\partial X} + U' \frac{\partial U'}{\partial Z} = 0 \qquad (A21)$$

$$\frac{\partial \eta}{\partial T} + U' \frac{\partial \eta}{\partial X} = -(1 + \eta) \frac{\partial U'}{\partial X} \qquad (A22)$$

Multiply equation (A22) by $f'(\eta)$ and add to equation (A21) where $f(\eta)$ is a function to be determined. Since

$$\frac{\partial f(\eta)}{\partial T} = f'(\eta) \frac{\partial \eta}{\partial T}$$

$$\frac{\partial f(\eta)}{\partial X} = f'(\eta) \frac{\partial \eta}{\partial X}$$

we find that

$$\left(\frac{\partial}{\partial T} + U'\frac{\partial}{\partial X}\right)(f'(\eta) + U') = -(1 + \eta) f'(\eta) \frac{\partial U'}{\partial X} - \frac{\partial \eta}{\partial X} \qquad (A23)$$

Assume that

$$(\eta + 1)(f'(\eta))^2 = 1 \tag{A24}$$

Therefore,

$$(\frac{\partial}{\partial T} + U' \frac{\partial}{\partial X})(f(\eta) + U') = -(1 + \eta)\, f'(\eta) \frac{\partial}{\partial X} [f(\eta) + U'] \tag{A25}$$

From equation (A14) we can determine $f(\eta)$ or

$$f'(\eta) = (\eta + 1)^{-1/2} \tag{A26}$$

Integrate equation (A26) from 0 to η. Note the indeterminate nature of the coefficient of integration, both $2((1 + \eta)^{1/2} - 1)$ and $2((1 + \eta)^{1/2} + 1)$ are solutions. Following Lamb (1932) we choose the negative sign. This boundary condition gives

$$f(\eta) = 2((1 + \eta)^{1/2} - 1) \tag{A27}$$

With the following definitions

$$P = f(\eta) + U'$$

$$Q = f(\eta) - U'$$

$$V' = (1 + \eta)\, f'(\eta)$$

we find that equation (A25) becomes

$$\frac{\partial P}{\partial X} + (U' + V') \frac{\partial P}{\partial X} = 0 \tag{A28}$$

This is a one-dimensional wave equation and P is a constant for a point moving with velocity U'+ V' in the positive direction. If we subtract equation (A21) from f'(η) times equation (A22) and follow the same procedure as for equation (A28), we find the corresponding wave equation for Q

$$\frac{\partial Q}{\partial T} + (U' - V') \frac{\partial Q}{\partial X} = 0 \qquad \text{(A29)}$$

Q is a constant for a point moving with velocity U' - V' in the negative direction. Given an initial disturbance after some small time the disturbance will separate into waves traveling in the positive and negative directions. Following the positve wave

$$Q = 0 = f(\eta) - U'$$

By definition

$$1/2P = f(\eta) = 2[(1 + \eta)^{1/2} - 1] = U' \qquad \text{(A30)}$$

Equation (A30) is valid as long as dispersion may be neglected. Since we are interested in the case where dispersion is important we may use equation (A30) as an initial condition for our problem. Note that this initial condition is not for the time equal to zero but for the time greater than zero when the effects of dispersion begin to be important. The above derivation comes from Lamb (1932) article 187.

APPENDIX II

Numerical Method of Solution

The equations describing an undular hydraulic jump are third-order non-linear partial differential equations. There is no analytic method available to solve this set of equations and therefore numerical methods must be used. However, even with numerical methods, some simplifications must be made to make the problem tractable. As a result, this work assumes that the Boussinesq equations force the sediment transport equation but the sediment transport equation has no effect on the jump equations. Solving the fully coupled set of equations results in such an unstable scheme as to be impractical.

The method used follows very closely work done by Peregrine (1966). We will use a predictor-corrector technique to solve equations (5) and (20) at each time and use the resulting mean velocity to drive the simple box model formulation of the sediment transport equation.

Equation (A5) is first written in discrete explicit form and solved for a provisional value of the surface height. In order to do this initial conditions must be specified at the previous time step. We use equation (A30) with an assumed surface profile that approximates the initial shape of the water surface that we expect. A function of the form

$$\eta = 1/2\ \eta_0\ (1 - \tanh\ (x/a)) \qquad (A31)$$

with

$$U' = 2\left((1 + \eta)^{1/2} - 1\right) \qquad A32)$$

where η_0 is the initial amplitude of the wave and "a" is the parameter controlling the slope of the wave face, the larger "a" is the more gentle the slope. The initial mean velocity U' is from equation (A30). These are the initial conditions for the following discrete form of equation (A5) (after Peregrine (1966))

$$\frac{\eta^*_{r,s+1} - \eta_{r,s}}{\Delta T} + U'_{r,s}\left(\frac{\eta_{r+1,s} - \eta_{r-1,s}}{2\Delta X}\right) + \left(1 + \frac{\eta^*_{r,s+1} + \eta_{r,s}}{2}\right)$$

$$\left(\frac{U'_{r,s+1} - U'_{r-1,s}}{2\Delta X}\right) = 0 \qquad (A33)$$

where r is the space step and s + 1 is the time step to be solved for. The known time step is denoted by s. Solving for $\eta^*_{r,s+1}$ for all r at s + 1 explicitly gives a value that can be used in the following discrete form of equation (A20)

$$\frac{U'_{r,s+1} - U'_{r,s}}{\Delta T} + \varepsilon U'_{r,s}\left(\frac{U'_{r+1,s+1} - U'_{r-1,s+1} + U'_{r-1,s} - U'_{r-1,s}}{4\Delta X}\right)$$

$$\frac{\eta^*_{r+1,s+1} - \eta^*_{r-1,s+1} + \eta_{r-1,s} - \eta_{r-1,s}}{4\Delta X} = 1/3\,\mu$$

$$\left[\frac{U'_{r+1,s-1} - 2U'_{r,s+1} + U'_{r-1,s+1} - U'_{r+1,s} + 2U'_{r,s} - U'_{r-1,s}}{\Delta X^2 \Delta T}\right]$$

(A34)

Solving this equation for the three unknowns $U'_{r-1,s+1}$, $U'_{r,s+1}$, $U'_{r+1,s+1}$ implicitly gives a tridiagonal matrix. This is the reason for choosing to discretize the equations in this way since we can use a modified Gauss technique to factor the matrix once and then solve directly for $U'_{r,s+1}$ for all r by back substitution. Solving one explicit equation and one tridiagonal equation is orders of magnitude faster than setting up both equations in a single matrix and solving the entire set simultaneously. Now that U' at the s+1 time step has been found for all r we use the result to find a final value for η with a discrete form of equation (A5)

$$\frac{\eta_{r,s+1} - \eta_{r,s}}{\Delta T} + (1 + \eta_{r,s}) \left(\frac{U'_{r+1,s+1} - U'_{r-1,s+1} + U'_{r+1,s} - U'_{r-1,s}}{4\Delta X}\right)$$

$$+ 1/2 \, (U'_{r+1,s+1} + U'_{r,s}) \left(\frac{\eta_{r+1,s} - \eta_{r-1,s}}{2\Delta X}\right) = 0 \qquad \text{(A35)}$$

We can solve equation (A35) explicitly for η. Now we have final values for both the mean velocity U' and the surface height at the s+1 time step for the entire range r. We can use these values both as initial conditions for the s+2 time step and as forcing functions for a discrete form of the sediment transport equation. Substitution of U' into the nondimensional form of equation (7) gives the nondimensional volume flux out of a box of length Δx and unit width and depth. Note that U_T is negative and so the sediment profile Z is therefore

$$Z_{r,s+1} = Z_{r,s} + U_{T_{r+1,s+1}} (\alpha U^2_{T_{r+1,s+1}} - \beta) \frac{\Delta T}{\Delta X} - U_{T_{r,s+1}}$$

$$(\alpha U_{T_{r,s+1}} - \beta) \frac{\Delta T}{\Delta X} \qquad \text{(A36)}$$

where $\alpha = \frac{K_T C_f \rho}{\rho_s}$ and $\beta = \frac{K_T \tau_c}{\rho_s g h_o}$.

There are two problems connected with numerical solutions of this type. They are the question of stability and effects of boundary conditions. Convergence is usually assumed for stable solutions. Neither problem is subject to simple analytic treatment. The question of ability of a third order nonlinear equation such as equation (A20) is simply not analytic. The only choice is to choose various mesh ratios of $\frac{\Delta T}{\Delta X}$, solve the set of equations and try to find a point where decreasing the mesh ratio does not change the results significantly. Considering the high order of the problem one must expect a small mesh ratio. Peregrine found that a mesh ratio of one was adequate while we found that one half was necessary for stable results. The difference is perhaps due to different opinions of what is a significant change between runs or the larger final time step reached in this case. A small mesh ratio means more computer time to reach a given time step. The question of boundary conditions is also connected to the problem of computer time.

In fact, the effects of an undular hydraulic jump are damped by

friction a large distance downstream from the jump. This means that the boundary conditions are effectively $\eta = 0$ at $x = -\infty$ and $\eta = 0$ at $x = \infty$. Practically we must truncate our range in the model. In so doing, we are specifying spurious "computational" boundary conditions that will effect the problem. A more complete discussion of this problem may be found in Chen (1973) or Bennett (1976). The effect of this problem is that the simplest set of boundary conditions has the effect of a rigid wall at either end of the model. These rigid walls reflect energy back into the system more or less completely and inevitably this will break down the model. Even rather complex boundary conditions reflect some portion of the energy. Boundary conditions that do not reflect energy can be derived for this model using the method of characteristics and radiation conditions but their complexity have computer time and computer storage requirements that approach those that would result from using large ranges and fixed boundaries (Bennett, 1976). However, large ranges mean large matrices and large run times. So the problem becomes one of choosing the largest mesh ratio consistent with stability and the smallest range consistent with avoiding reflections in the time we are interested in. Unfortunately the only way to make these decisions is to actually run the program and see what happens.